Multi-core Fiber for High-Capacity Long-Haul Spatially-Multiplexed Transmission

Tetsuya HAYASHI*, Toshiki TARU, Takuji NAGASHIMA, Osamu SHIMAKAWA, Takashi SASAKI and Eisuke SASAOKA

Data traffic is growing exponentially due to the emergence of various network services. Although the transmission capacity of optical fibers has dramatically increased thanks to advanced communication technologies such as wavelength-division multiplexing and multi-level modulation, the capacity is rapidly approaching its fundamental limit as the amplification bandwidth has been used up and drastic improvements of the signal-to-noise ratio cannot be expected any further. To overcome this problem, space-division multiplexing has come to attract lots of attention, and we have conducted research and development on multi-core fiber (MCF), achieving positive results. This paper reviews the major achievements of our MCF research and development.

Keywords: optical fiber communication, space-division multiplexing, spatial multiplexing, multi-core fiber, inter-core crosstalk

1. Introduction

Data traffic is growing exponentially due to the emergence of various network services such as video streaming and smartphones. The transmission capacity of the optical fiber has also been increasing exponentially due to the roll-outs of technologies such as wavelength-division multiplexing (WDM)[*1] and the multi-level modulation[*2]; however, the capacity is rapidly approaching its fundamental limit due to the depletion of the amplification bandwidth[*3] and the limit of signal-to-noise ratio (SNR) from nonlinear noise[*4] [1],[2]. Under these circumstances, space-division multiplexing (SDM) has come to attract a lot of attention[2],[3]. For further increasing fiber capacity, various research groups have been investigating SDM-related technologies.

For overcoming the capacity limit, we have been promoting research and development on multi-core fiber (MCF) toward practical use. Since the MCF includes the plurality of cores as shown in **Fig. 1**, characteristics degradations specific to the MCF structure, which were not observed in the conventional single-core fiber (SCF), are concerns for the actualization of this technology. The inter-core crosstalk (XT) is one of the most important parameters in the MCF, and suppression of the XT is crucial for transmitting signals independently on individual cores. We proposed and experimentally validated a theoretical model that can predict the crosstalk and its statistical characteristics of actual MCFs[4]-[7], demonstrated that low loss and ultra-low XT—necessary for long-haul transmission—can be achieved in the fabricated MCF[6]-[8], theoretically revealed the behavior of the XT as a noise[8]-[10], and enhanced the SNR of each core of the MCF based on considering the XT as a noise[11],[12], each for the first time. This paper reviews these major achievements of our research and development on the MCF.

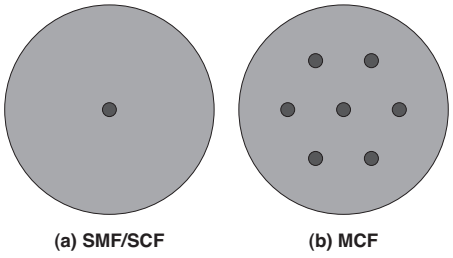

Fig. 1. Schematic cross sections of optical fibers (Darker color represents higher refractive index)

2. Behavior of Inter-core Crosstalk

2-1 Theoretical prediction in earlier studies

Earlier studies[13]-[15] reported that the XT of the MCF can be suppressed by inducing a slight difference in the effective refractive indices (n_{eff}s) between cores, based on theoretical considerations. According to these studies, the XT from Core m to Core n can be expressed by using the coupled-mode equation[16]:

$$\frac{dA_n}{dz} = -j\kappa_{nm} \exp\left[j\left(\beta_n - \beta_m\right)z\right] A_m , \quad \cdots\cdots (1)$$

where A_n is the complex amplitude of the electric field of Core n, κ_{nm} is the mode-coupling coefficient from Core m to Core n, $\beta_n = (2\pi/\lambda)\, n_{\mathrm{eff},n}$ is the propagation constant of Core n, and z is the longitudinal position along the fiber. When only Core m is excited [$A_m(0) = 1$], the power of Core n can be derived as[16]:

$$|A_n|^2 = F \sin^2 qz , \quad \cdots\cdots (2)$$

$$F = \left[1 + \left(\frac{\beta_n - \beta_m}{2\kappa_{nm}}\right)^2\right]^{-1}, \quad q = \sqrt{\kappa_{nm}^2 + \left(\frac{\beta_n - \beta_m}{2}\right)^2} . \quad \cdots\cdots (3)$$

Thus, a slight difference in n_{eff} can remarkably suppress the maximum power transfer ratio F, as shown in **Fig. 2**. This

is because the slight difference in n_{eff} can induce a large difference in β in conditions of $\lambda \sim 10^{-6}$, and the large variation of the phase difference along the MCF—the phase mismatch— inhibits efficient mode couplings.

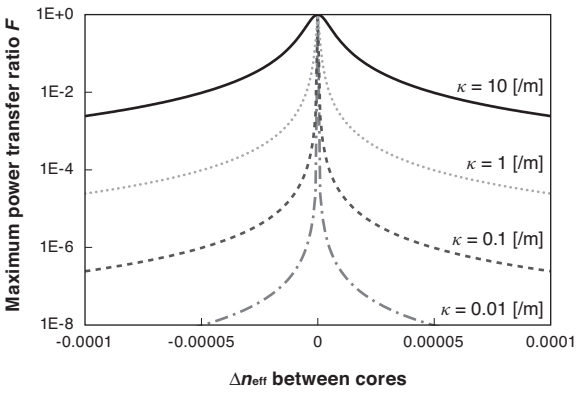

Fig. 2. The relationship between the inter-core refractive index mismatch and the power conversion efficiency F at 1550 nm

2-2 Effect of fiber bend on the crosstalk

However, the above discussion is based on the simple coupled-mode theory that assumes ideal conditions where the cores are not longitudinally perturbed, and thus was anticipated to be inapplicable to actual MCFs, which are longitudinally perturbed by various internal and external factors. We speculated that the fiber bend should have a particularly large effect on the XT, and therefore investigated the effect theoretically and experimentally[4].

Based on the equivalent index model[17], which has been widely used in loss analysis of bent waveguides, a bent fiber can be described as a corresponding straight fiber which has an equivalent refractive-index profile

$$n_{\mathrm{eq}} \approx n_{\mathrm{mat}}\left(1+\frac{r\cos\theta}{R_{\mathrm{b}}}\right), \quad \cdots\cdots (4)$$

where n_{mat} is the intrinsic refractive index of the material, R_{b} is the bend radius, and (r, θ) is the local polar coordinate on the fiber cross-section (see **Fig. 3**). The equivalent effective index of the Core n of an MCF can be expressed as

$$n_{\mathrm{eff},n} \approx n_{\mathrm{eff},n}\left(1+\frac{r_n\cos\theta_n}{R_{\mathrm{b}}}\right). \quad \cdots\cdots (5)$$

Equation (5) may be intuitively understood as such that the change of the optical path length due to the bend is simply translated into the change of the refractive index, although it is not a rigorous interpretation. By assuming, for explanation simplicity, that Core m is the center core and the distance between the centers of Core m and Core n is D_{nm}, a slight difference in n_{eff} between the cores can be nagated, as shown in **Fig. 3,** by the fiber bend when the bend radius is no more than the threshold bend radius R_{pk}:

$$R_{\mathrm{pk}} = \frac{n_{\mathrm{eff},n}}{\left|n_{\mathrm{eff},m} - n_{\mathrm{eff},n}\right|} D_{nm}, \quad \cdots\cdots (6)$$

and the XT is considered to be largely degraded.

In order to quantify the effect of the bend on the XT, we theoretically and experimentally investigated the dependence of the XT on the bend radius. If the propagation constants are variable along propagation distance z, the coupled-mode equation can be expressed as

$$\frac{dA_n}{dz} = -j\kappa_{nm}\exp\left[j\int_0^z\left(\beta_{\mathrm{eq},n}-\beta_{\mathrm{eq},m}\right)dz'\right]A_m \quad \cdots\cdots (7)$$

where $\beta_{\mathrm{eq},n} = (2\pi/\lambda)\, n_{\mathrm{eff,eq},n}$ is the equivalent propagation constant. **Figure 4** shows an example of longitudinal evolutions of XT—to be precise, coupled power, or $|A_n|^2$ calculated using **Eq. (7)** — and equivalent effective indices

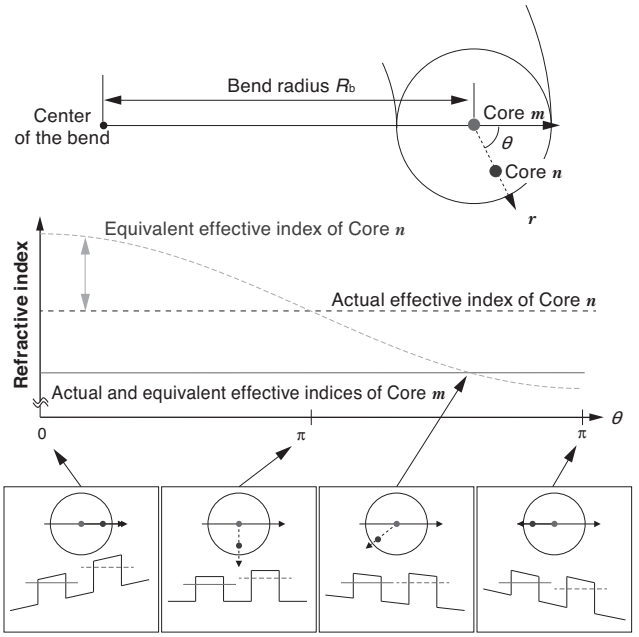

Fig. 3. Variation of the equivalent refractive index due to the fiber bend

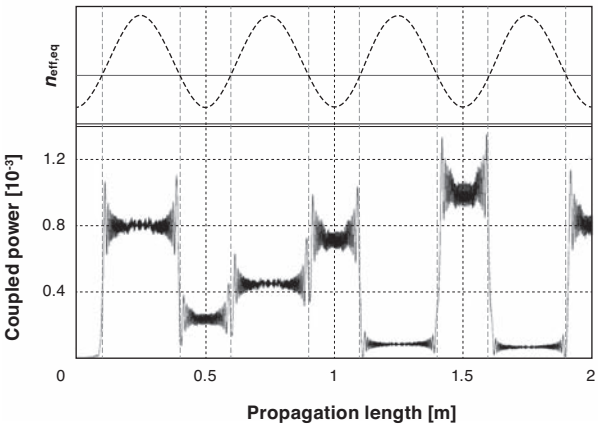

Fig. 4. Example of longitudinal evolutions of a calculated coupled power and equivalent effective indices between the two cores, in the case where the MCF is bent at a constant bend radius ($R_{\mathrm{b}} < R_{\mathrm{pk}}$) and twisted at the constant rate of 2 turns/m

between the two cores, in the case where the MCF is bent at a constant bend radius ($R_b < R_{pk}$) and twisted at the constant rate of 2 turns/m. In contrast with the simple oscillation shown in **Eqs. (2) and (3)**, the XT changed dominantly at every phase-matching point where the equivalent effective indices are equal, and the changes appear random. Only little oscillations occurred in XT at positions other than the phase-matching points.

The reason why the dominant XT changes appear random is because the phase differences between the cores are different for each phase-matching point. In the calculation, these random changes are deterministic; however, they are considered to be stochastic in practice because the phase differences can be easily fluctuated in practice by slight variations in the bending radius, twist rate of fiber, and so on. Therefore, to deal with such randomness of the XT, we conducted a Monte Carlo simulation by introducing random phase shifts to **Eq. (7)**, and investigated the relationship between the bend radius and statistical mean of the simulated XT. In addition, we evaluated a fabricated MCF, and validated the above consideration and simulation method. Comparisons between the measured and the simulated XT are shown in **Fig. 5**. Points represent the averages of ten measurements under the same conditions, and the MCF was rewound before each of the ten measurements. The error bars indicate the maximum and the minimum of the measured values at each bend radius. The solid line represents the average of the simulated XT for 600 instances. The measured and the simulated XT are in a good agreement. From these results, we revealed that the measured XT can be predicted by the theoretical model. Fiber designs considering the effect of the bend are necessary for the XT suppression in MCFs[4].

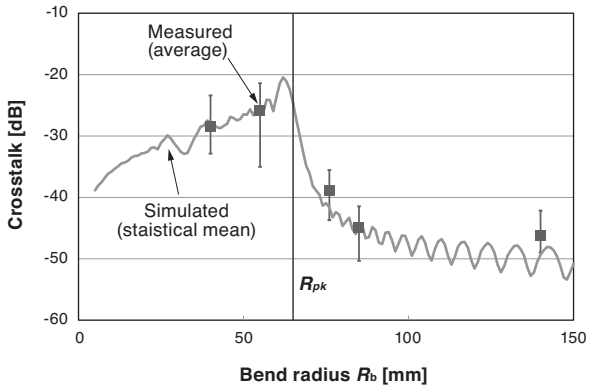

Fig. 5. Example of the dependence of the crosstalk on the bend radius

2-3 The crosstalk of the homogeneous MCF

Based on the previous section, it was found that the XT can be suppressed if R_b is adequately larger than R_{pk}, and large differences in the optical properties between the cores are required to shorten R_{pk}. On the other hand, it is unfavorable to pack different types of cores into an MCF because the characteristics of every core of the MCF transmission lines need to be managed. Therefore, we proposed a low-XT homogeneous MCF, where all the cores are identical, by utilizing the bend for inducing the phase mismatch[5]-[8].

In this section, we review the derivation and validation of the analytical expressions of the statistical characteristics of the XT of the homogeneous MCF, with which we can easily design homogeneous MCFs.

If the bend perturbation is dominant, the XT discretely changes at every phase-matching point, as shown in **Fig. 4**. These XT changes can be approximated as discrete and random mode coupling:

$$A_{n,N} = A_{n,N-1} - jK_{nm,N} \exp(j\varphi_{\mathrm{rnd},N})\, A_{m,N-1}\,, \quad \cdots\cdots (8)$$

where $A_{n,N}$ is the A_n after N-th phase-matching point, $\varphi_{\mathrm{rnd},N}$ the phase difference between the cores at N-th phase-matching point, and $K_{nm,N}$ the *coupling coefficient* from Core m to Core n for the discrete change. The phase difference $\varphi_{\mathrm{rnd},N}$ is a random number as we mentioned above. If only Core m is excited ($A_{m,0} = 1$, $A_{n,0} = 0$), by assuming adequately low XT, the approximations of $|A_{n,N}| \ll 1$ and $A_{m,N} \approx A_{m,0} = 1$ hold, and the XT value X can be approximated as $|A_{n,N}|^2$. Thus, **Eq. (8)** can be approximated as

$$A_{n,N} \approx -j\sum_{l=1}^{N} K_{nm,l} \exp(j\varphi_{\mathrm{rnd},l})\,. \quad \cdots\cdots (9)$$

The probability density functions (PDFs) of $\Re[K_{nm}\exp(j\varphi_{\mathrm{rnd}})]$ and $\Im[K_{nm}\exp(j\varphi_{\mathrm{rnd}})]$ are not normally distributed; however, based on the central limit theorem, the PDFs of $\Re[A_{n,N}]$ and $\Im[A_{n,N}]$ can converge to a normal distribution if N is large enough. With some assumptions, the variance of $\Re[A_{n,N}]$s and $\Im[A_{n,N}]$s of the two polarization modes can be analytically derived as[7]:

$$\sigma^2_{4\mathrm{df}} \approx \frac{1}{2}\,\kappa^2_{nm}\,\frac{\lambda R_b}{2\pi n_{\mathrm{eff},n} D_{nm}}\,L\,, \quad \cdots\cdots (10)$$

where L is the fiber length. Since the sum of powers of l random numbers—whose PDFs are the standard normal distribution— has the PDF of the chi-square distribution with l degrees of freedom (df), the PDF of X ($\approx |A_{n,N}|^2 = \{\Re[A_{n,N}]\}^2 + \{\Im[A_{n,N}]\}^2$) can be expressed as[7]

$$f(X) = \frac{X}{4\sigma^4_{4\mathrm{df}}}\exp\left(-\frac{X}{2\sigma^2_{4\mathrm{df}}}\right), \quad \cdots\cdots (11)$$

and the mean value (mean XT) of X can be expressed as

$$\mu_{X,nm} \approx 4\sigma^2_{4\mathrm{df}} \approx \kappa^2_{nm}\,\frac{\lambda R_b}{\pi n_{\mathrm{eff},n} D_{nm}}\,L\,. \quad \cdots\cdots (12)$$

It can be found, from **Eq. (12)**, that the XT can be suppressed by shortening the bend radius R_b. In decibels, 99.99 percent of the XT distribution is μ_X + ~7.7 dB—the XT distribution on the decibel scale has the constant shape independent of μ_X.

The XT distribution expressed by **Eq. (11)** can be measured with the wavelength scanning method[8]. The XT value X can be adequately dispersed by the randomization of the phase difference between cores, thanks to the wavelength dependence of the propagation constant. A measured XT spectrum is shown in **Fig. 6**, and the XT distribution ob-

tained from the data of **Fig. 6** is shown in **Fig. 7**. It can be observed that *X* heavily varied with wavelength and that the actual XT distribution is well fitted by **Eq. (11)**.

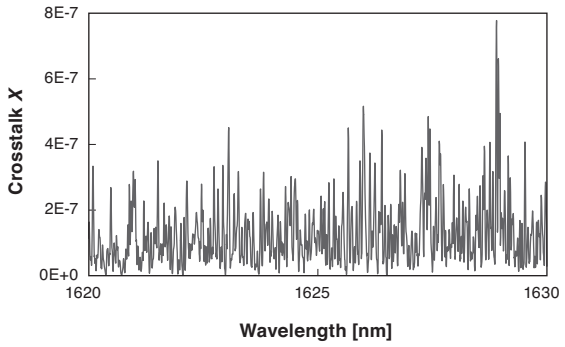

Fig. 6. Example of the XT spectrum

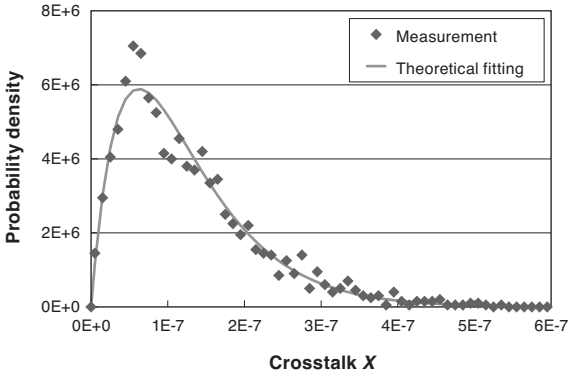

Fig. 7. Example of the XT distribution

3. Demonstration of Ultra-Low-Crosstalk Homogeneous MCF Feasible to Long-Haul Transmission

We designed and fabricated a low-XT homogeneous MCF (MCF-A) by using **Eqs. (11) and (12)**[5]-[8].

Figure 8 shows a cross section of the fabricated MCF-A. The core pitch, the cladding diameter, and the coating diameter of MCF-A were 45 μm, 150 μm, and 256 μm, respectively. **Table 1** shows the optical properties of each MCF-A core. The transmission loss was 0.175–0.181 dB/km (avg. 0.178 dB/km) at 1550 nm, and no more than 0.192–0.202 dB/km in C+L band (1530–1625 nm), owing to the pure silica core technology. Furthermore, no loss degradations were observed in the outer cores. Including other optical properties, the fabricated MCF was suitable for C+L band transmission that is necessary for long-haul transmission.

Figure 9 shows the mean XT between neighboring cores of MCF-A, measured using the wavelength scanning method[8]. The measurement results were in good agreement with **Eq. (12)**. The averages of the mean XT μx were

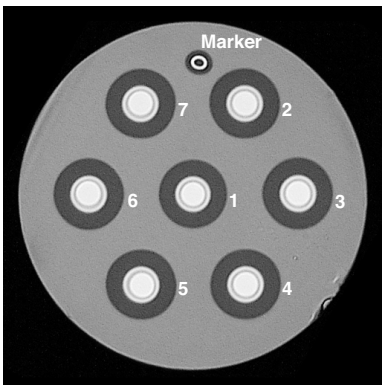

Fig. 8. A cross section of MCF-A

Table 1. Optical properties of cores of MCF-A

	Transmission loss [dB/km]	λ_{cc} [nm]	MFD [μm]	A_{eff} [μm^2]	Disp. [ps/(nm·km)]	D. slope [ps/(nm^2·km)]
λ [nm]	1550 1625		1550	1550	1550	1550
Avg.	0.178 0.198	1497	9.8	79.9	22.2	0.062
Min.	0.175 0.192	1483	9.7	78.2	22.1	0.062
Max.	0.181 0.202	1509	9.9	81.3	22.2	0.062

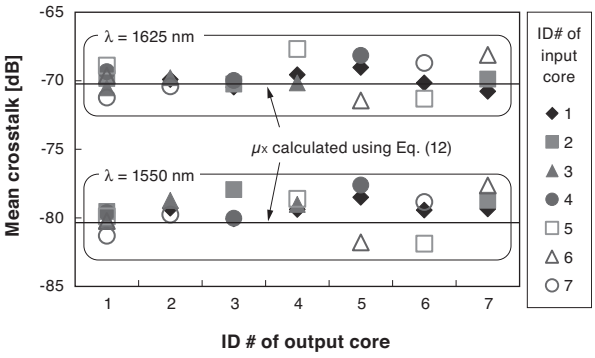

Fig. 9. Mean crosstalk between neighboring cores of MCF-A after 17.4-km propagation

as low as −79.5 dB at 1550 nm, and −69.7 dB at 1625 nm. Even μx from 6 outer cores to the center core (center-core μx) was −72.3 dB at 1550 nm, and −62.1 dB at 1625 nm.

By using **Eq. (12)**, the dependence of μx on the propagation length L and the bend radius R_b can be estimated, though the length and the bend radius of MCF-A was 17.4 km and 140 mm, respectively. **Figure 10** shows the relationship between the propagation length, the bend radius, and the center-core μx of MCF-A at 1550 nm. The center-core μx and the 99.99 percent of the XT can be less than −30 dB, even after 10,000 km when R_b is less than ~4 m and ~0.7 m respectively, and it was demonstrated for the first time that the XT of the MCF can be suppressed enough for ultra-long-haul transmission.

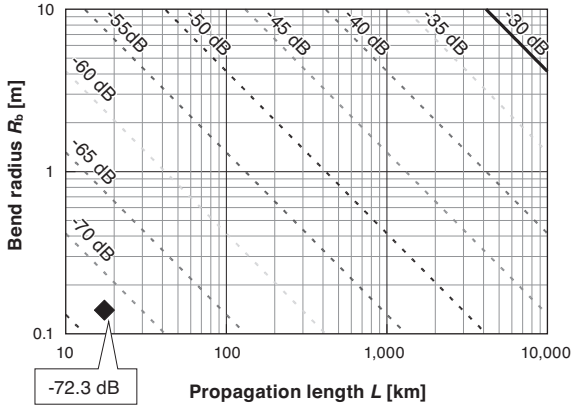

Fig. 10. The relationship between the propagation length, the bend radius, and the mean XT μ_X to the center core of MCF-A at 1550 nm. Diamond: R_b and L where μ_X was measured. Contour lines represent μ_X to the center core, estimated from the measurement values and Eq. (12).

With this MCF, a transmission capacity of more than 100 Tb/s per fiber was achieved, for the first time, in the transmission experiment conducted by The National Institute of Information and Communications Technology, among others[18), 19)].

4. Effect of the Crosstalk on the Transmission Quality

In the previous section, the target level of the XT was set such that the 0.9999-quantile of the statistical distribution should be less than −30 dB, after an earlier study[15)], which set the target of the XT between neighboring cores as less than −30 dB. However, it was not necessarily based on theoretical groundings, which should include the consideration of the behavior of the XT as a noise. Therefore, we considered the effect of the XT on the transmission quality[9),10)], based on the stochastic behavior of the XT, which are described in the previous section.

Based on Section 2, the XT of the MCF stochastically changes with the time/wavelength variation of the phase difference between the cores, and the I- and Q-components[*5] of the two polarization modes of coupled light (XT light) are normally distributed with the variance of $\mu_X/4$. Like amplified spontaneous emission (ASE) noise[21)] and nonlinear interference noise[22)], XT can be regarded as a virtual additive white Gaussian noise when the bandwidth of the signal light is adequately broad, since the XT changes rapidly in the wavelength.

The Q-factor—that is, the most commonly used figure of the transmission quality— can be defined as[22)]:

$$Q = \frac{|\mu_1 - \mu_2|}{\sigma_1 + \sigma_2} \quad \cdots\cdots (13)$$

where μ_i and σ_i are the means and the standard deviations, respectively, of the neighboring constellation points.

The decibel value of the Q-factor can be expressed as

$$Q_{\mathrm{dB}} = 20\log_{10} Q = 10\log_{10} Q^2 . \quad \cdots\cdots (14)$$

Therefore, hereinafter, we will discuss the Q^2-factor instead of the Q-factor. If we assume $\sigma_n = \sigma_1 = \sigma_2$, and let $S = |\mu_1 - \mu_2|$, the nearest distance between the constellation symbols, the Q^2-factor, can be expressed as

$$Q_n^2 = \frac{S^2}{4\sigma_n^2} . \quad \cdots\cdots (15)$$

When we consider the total mean XT $\mu_{X,\mathrm{total}}$ from other cores, where the mean XT is defined as the average power of the XT light divided by that of the signal power P_s, the variance σ_x^2 of the XT light on the I–Q planes can be expressed as

$$\sigma_x^2 = P_s \frac{\mu_{X,\mathrm{total}}}{4} . \quad \cdots\cdots (16)$$

Since the variance of a sum of statistically independent variables equals to the sum of the variances of the statistically independent variables, the Q^2-factor affected by the XT can be expressed as

$$Q_x^2 = \frac{S^2}{4(\sigma_n^2 + \sigma_x^2)} . \quad \cdots\cdots (17)$$

From **Eqs. (15)–(17)**, XT-induced Q^2-penalty (Q_n^2/Q_x^2) can be expressed as

$$\frac{Q_n^2}{Q_x^2} = 1 + Q_n^2 \mu_{X,\mathrm{total}} \frac{P_s}{S^2} = \left(1 - Q_x^2 \mu_{X,\mathrm{total}} \frac{P_s}{S^2}\right)^{-1} , \cdots (18)$$

where P_s/S^2 is the value determined by the modulation format. Values of P_s/S^2 for typical ideal modulation formats are shown in **Table 2**. **Figure 11** shows the XT-induced Q^2-penalty at $Q_x^2 = 9.8$ dB (bit-error rate BER = 1×10^{-3}), which was calculated using **Eq. (18)**. The XT-induced Q^2-penalty (Q_n^2/Q_x^2) can be suppressed to be less than 1 dB at $Q_x^2 = 9.8$ dB if $\mu_{X,\mathrm{total}}$ can be suppressed to be less than −16.7 dB for PDM-QPSK, −23.7 dB for PDM-16QAM, and −29.9 dB for PDM-64QAM.

This result revealed that signals modulated with a high-order modulation with a spectral efficiency (SE) of 10 bit/s/Hz or more can be transmitted with no significant penalty if $\mu_{X,\mathrm{total}}$ is less than about −30 dB after the propagation of the total MCF link, and that MCF-A can transmit the high-SE signals over ultra-long-haul (> 10,000 km) links in terms of the XT.

Table 2. Values of P_s/S^2 for the typical modulation format

Modulation format	P_s/S^2
PDM-QPSK	1
PDM-8PSK	$2^{1/2} / (2^{1/2}-1)$
PDM-16QAM	5
PDM-32QAM	10
PDM-64QAM	21
PDM-128QAM	41

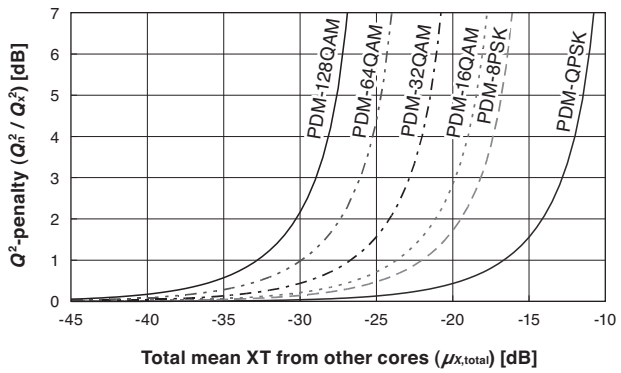

Fig. 11. XT-induced Q^2-penalty at $Q_{w/XT}^2$ = 9.8 dB

5. Enhancement of SNR in MCF

Though the XT of MCF-A was confirmed to be extremely low, the suppression of noises other than the XT is also very important for long-haul transmission.

Recently, owing to the actualization of digital coherent detection, the phase information of light can be received, and linear distortions—such as the chromatic dispersion—can be compensated by digital signal processing. Therefore, the suppression of the ASE noise and the nonlinear interference (NLI) noise has become one of the most important issues for the SCF for high-capacity transmission[2], and a recent high-capacity transmission experiment has employed an SCF that has low loss for ASE noise suppression and large effective area A_{eff} for NLI noise suppression[23].

The XT of MCF-A was suppressed to an extremely low level; however, the transmission loss was higher than that of typical pure-silica-core SCF (≤ 0.17 dB/km)—though it was lower than that of the standard SMF (SSMF) and the lowest in reported MCFs, and A_{eff} was not improved from SSMF. Therefore, we proposed an MCF that can suppress the ASE and NLI noises by lowering loss and enlarging A_{eff} and can *properly* suppress the XT simultaneously[11],[12].

5-1 Effect of crosstalk on SNR

For the single-core dispersion-uncompensated Nyquist WDM[*6] transmission system, SNR can be estimated using closed-form equations[21], and the maximum SNR achievable in the system (SNR_{SC}: the SNR includes ASE and NLI noises but does not include XT) can be derived.

As described in Section 4, when the bandwidth of the signal light is adequately broad, XT can be regarded as a virtual additive white Gaussian noise, similar to ASE and NLI noises. Accordingly, the maximum SNR achievable in the multi-core system (SNR_{MC}: the SNR includes ASE, NLI, and XT noises) can be derived[11],[12], by expanding the equations in Ref. (21). From the derived expressions, it was found that the XT-induced SNR penalty (SNR_{SC}/SNR_{MC}) is dependent on the noise figure F of optical amplifiers, the whole bandwidth B_{WDM} of WDM, and the span length (interval of the amplifiers), but independent of the number of spans, or (the length of transmission link) = (the span length) × (the number of spans). This is because F, B_{WDM}, and the span length affect the ratio of ASE/NLI noise increase per unit length to the XT increase per unit length, but the number of spans does not affect the ratio.

Figure 12 shows the XT-induced SNR penalty in the MCF with SSMF cores (loss ~ 0.19 dB/km, A_{eff} ~ 80 μm²) at a wavelength of 1550 nm in the condition at the span length of 80 km. It was found that the SNR penalty begins to drastically degrade when $\mu_{X,total}$ per one 80-km span exceeds 10^{-4} (−40 dB), and that the effect of over suppression of the XT is limited.

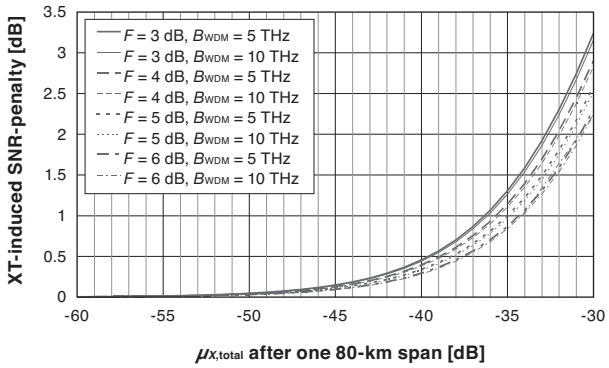

Fig. 12. XT-induced SNR penalty in the MCF with SSMF cores (A_{eff} ~ 80 μm²). (F: the noise figure of optical amplifier, B_{WDM}: the whole bandwidth of WDM)

5-2 Fabrication of the low-loss large-A_{eff} low-XT MCF

$\mu_{X,total}$ of MCF-A was about −66 dB at 1550 nm after 80-km propagation, and it can be noted that the $\mu_{X,total}$ was suppressed *too much* in terms of the suppression of the XT-induced SNR penalty. Thus, by relaxing the target of $\mu_{X,total}$ such as less than −40 dB after 80-km propagation and leveraging the relaxed margin for enlarging A_{eff} of each core, we designed and fabricated an MCF (MCF-B) that can simultaneously achieve low loss, large A_{eff}, and low XT.

Figure 13 shows a cross-section of the fabricated MCF-

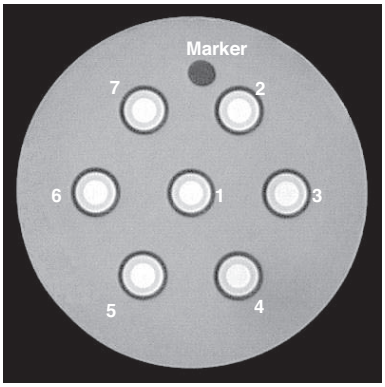

Fig. 13. A cross-section of MCF-B

B. Measured optical properties of MCF-B are shown in **Table 3** and in **Figs. 14 and 15**. The transmission loss we achieved was 0.163–0.172 dB/km (average: 0.168 dB/km) at 1550 nm, and no more than 0.183–0.194 dB/km over the whole C+L band, which are the lowest values among the reported MCFs. The A_{eff}s were 121–127 μm^2 (average: 124.1 μm^2). The core pitch and the cladding diameter of MCF-B were 51 μm and 188 μm. The μ_X between the neighboring cores were from −62.8 dB to −59.2 dB (average: −61.3 dB) for L = 6.99 km and R_b = 140 mm at λ = 1550 nm, and the center-core μ_X was −53.1 dB. Accordingly, the center-core μ_X was estimated to be −42.5 dB after 80-km propagation.

Table 3. Optical properties of cores of MCF-B

	Transmission loss [dB/km]	λ_{cc} [nm]	MFD [μm]	A_{eff} [μm^2]	Disp. [ps/(nm·km)]	D. slope [ps/(nm^2·km)]
λ [nm]	1550 1625		1550	1550	1550	1550
Avg.	0.168 0.188	1462	12.2	124.1	21.7	0.063
Min.	0.163 0.183	1457	12.1	121.3	21.7	0.062
Max.	0.172 0.194	1470	12.4	126.9	21.7	0.063

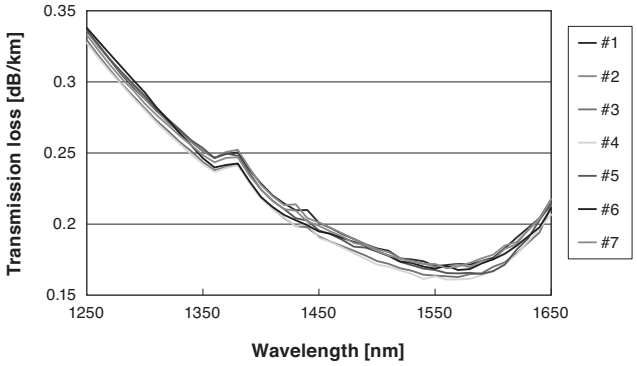

Fig. 14. Attenuation spectra of cores of MCF-B

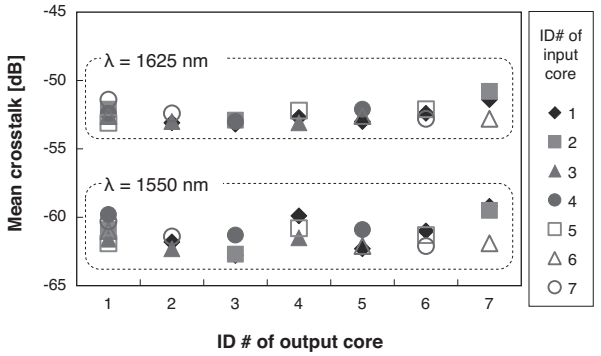

Fig. 15. Mean crosstalk between neighboring cores of MCF-B after 6.99-km propagation

5-3 SNR improvements of the fabricated MCFs from standard SMF

Figure 16 shows the calculated results how the XT-induced SNR penalty (SNR_{SC}/SNR_{MC}, shown as dash-dotted lines) and the SNR improvement (SNR_{MC}, shown as solid curves) from the standard SMF depend on SNR_{SC} and $\mu_{X,total}$ after one span, for MCF-A and MCF-B (see Ref. (12) for the details of the calculations). The calculation assumed a whole WDM bandwidth of 10 THz, noise figure of amplifiers of 4 dB, and a span length of 80 km. The SNR improvement and penalty, represented by the contour lines, are independent of the number of spans, as mentioned above. It can be seen that the SNR improvement by ASE/NLI noise suppression is cancelled if $\mu_{X,total}$ is larger than around −40 dB after 80-km propagation. It was confirmed that the SNR in each core was successfully improved in MCF-B by the design change from MCF-A to MCF-B, which leveraged the margin of the over suppressed XT of MCF-A for enlarging A_{eff} (and by lowering loss). Thus, it was revealed that balanced improvements of A_{eff}, transmission loss, and XT are important. The balance of A_{eff} and XT is especially important because A_{eff} enlargement weaken the power confinements into cores.

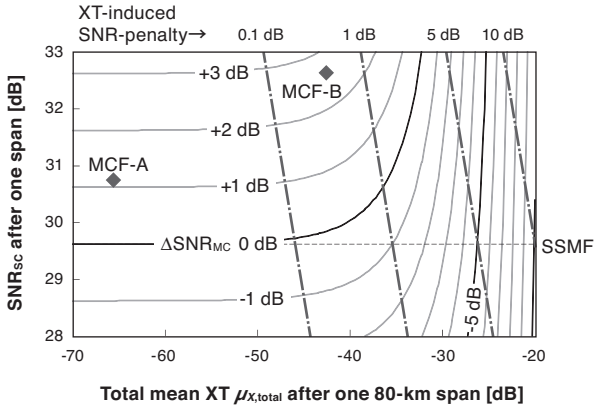

Fig. 16. SNR improvements of the fabricated MCFs compared with the standard SMF

6. Conclusion

We reviewed the major achievements of our research and development on the MCF. By investigating the behavior of the inter-core crosstalk (XT)—which does not occur in the conventional single-core fiber— in detail, we proposed and validated the simulation model that can predict the XT of actual MCFs, demonstrated the low-loss ultra-low-XT MCF feasible for ultra-long-haul high-capacity transmission by trial fabrication—the first > 100-Tb/s/fiber transmission experiment was conducted using the fabricated MCF. We also theoretically revealed the behavior of the XT as a noise, and improved the SNR of each core of the MCF even under the existence of the XT.

7. Acknowledgments

The research reviewed in this paper was supported in part by the National Institute of Information and Communications Technology (NICT), Japan under "Research on Innovative Optical Fiber Technology."

Technical Terms

*1 Wavelength-division multiplexing (WDM): A transmission technique that multiplexes signals on different wavelength channels, so that the transmission capacity per fiber can increase.

*2 Multi-level modulation: A modulation method that modulates intensity, amplitude, and/or phase of light in multiple level, so that bits-per-symbol can increase.

*3 The depletion of the amplification bandwidth: Recent high-capacity long-haul optical fiber transmission experiments utilize C+L band (1530–1625 nm) where the loss of silica glass is very low and the high-gain low-noise optical amplifiers are available; however, the C+L band is already used up in the recent experiments. Other wavelength bands are difficult to utilize because of the higher loss of optical fibers and of the higher noise or lower gain of optical amplifiers.

*4 Nonlinear interference noise: The noise due to the nonlinear interference that is induced by the interaction of high-intensity light and dielectric. In WDM, high-intensity wavelength channels may induce noises in different channels.

*5 I component, Q component, and I–Q plane: The amplitude and phase of the light can be expressed by in-phase (I) and quadrature (Q) components. The real and imaginary parts of the complex amplitude correspond to the I and Q components, respectively. I–Q plane is the plane with I and Q axes (corresponding to the complex plane for the complex amplitude).

*6 Nyquist WDM: The WDM technique that can realize the channel spacing equivalent to the symbol rate with no inter-channel interference without any guard band by the Nyquist filtering on each optical frequency channel.

References

(1) E. B. Desurvire, "Capacity demand and technology challenges for lightwave systems in the next two decades," J. Lightwave Technology, vol. 24, no. 12, pp. 4697–4710, 2006.
(2) R.-J. Essiambre and R. W. Tkach, "Capacity Trends and Limits of Optical Communication Networks," Proc. IEEE, vol. 100, no. 5, pp. 1035–1055, 2012.
(3) T. Morioka, "New generation optical infrastructure technologies: 'EXAT initiative' towards 2020 and beyond," in OptoElectron. Commun. Conf. (OECC), Hong Kong, 2009, paper FT4.
(4) T. Hayashi et al., "Crosstalk variation of multi-core fibre due to fibre bend," in Eur. Conf. Opt. Commun. (ECOC), 2010, paper We.8.F.6.
(5) T. Hayashi et al., "Low-crosstalk and low-loss multi-core fiber utilizing fiber bend," in Opt. Fiber Commun. Conf. (OFC), 2011, paper OWJ3.
(6) T. Hayashi et al., "Ultra-low-crosstalk multi-core fiber feasible to ultra-long-haul transmission," in Opt. Fiber Commun. Conf. (OFC), 2011, paper PDPC2.
(7) T. Hayashi et al., "Design and fabrication of ultra-low crosstalk and low-loss multi-core fiber," Opt. Express, vol. 19, no. 17, pp. 16576–16592, 2011.
(8) T. Hayashi et al., "Characterization of Crosstalk in Ultra-Low-Crosstalk Multi-Core Fiber," J. Lightwave Technol., vol. 30, no. 4, pp. 583–589, 2012.
(9) T. Hayashi et al., "Effects of inter-core crosstalk in multi-core fiber on Q-factor (in Japanese with English abstract)," IEICE Tech. Rep., vol. 112, no. 193, OCS2012-34, pp. 31–36, 2012.
(10) T. Hayashi et al., "Behavior of inter-core crosstalk as a noise and its effect on Q-factor in multi-core fiber," submitted for publication.
(11) T. Hayashi et al., "Low-Loss and Large-A_{eff} Multi-core Fiber for SNR Enhancement," in Eur. Conf. Opt. Commun. (ECOC), 2012, paper Mo.1.F.3.
(12) T. Hayashi et al., "Uncoupled multi-core fiber enhancing signal-to-noise ratio," Opt. Express, vol. 20, no. 26, pp. B94–B103, 2012.
(13) G. Le Noane et al., "Ultra high density cables using a new concept of bunched multicore monomode fibers: A key for the future FTTH networks," in Int. Wire Cable Symp. (IWCS), 1994, pp. 203–210.
(14) S. Kumar et al., "Optical fibers having cores with different propagation constants, and methods of manufacturing same," U.S. Patent 6611648, 26-Aug-2003.
(15) M. Koshiba et al., "Heterogeneous multi-core fibers: proposal and design principle," IEICE Electron. Express, vol. 6, no. 2, pp. 98–103, 2009.
(16) A. W. Snyder, "Coupled-Mode Theory for Optical Fibers," J. Opt. Soc. Am., vol. 62, no. 11, pp. 1267–1277, 1972.
(17) D. Marcuse, "Influence of curvature on the losses of doubly clad fibers," Appl. Opt., vol. 21, no. 23, pp. 4208–4213, 1982.
(18) J. Sakaguchi et al., "109-Tb/s (7×97×172-Gb/s SDM/WDM/PDM) QPSK transmission through 16.8-km homogeneous multi-core fiber," in Opt. Fiber Commun. Conf. (OFC), 2011, paper PDPB6.
(19) J. Sakaguchi et al., "Space Division Multiplexed Transmission of 109-Tb/s Data Signals Using Homogeneous Seven-Core Fiber," J. Lightwave Technol., vol. 30, no. 4, pp. 658–665, 2012.
(20) R.-J. Essiambre et al., "Capacity Limits of Fiber-Optic Communication Systems," in Opt. Fiber Commun. Conf. (OFC), 2009, paper OThL1.
(21) P. Poggiolini et al., "Analytical Modeling of Nonlinear Propagation in Uncompensated Optical Transmission Links," IEEE Photon. Technol. Lett., vol. 23, no. 11, pp. 742–744, 2011.
(22) "ITU-T Recommendation G.975.1." Feb-2004.
(23) A. Sano et al., "102.3-Tb/s (224 x 548-Gb/s) C-and extended L-band all-Raman transmission over 240 km using PDM-64QAM single carrier FDM with digital pilot tone," in Opt. Fiber Commun. Conf. (OFC), 2012, paper PDP5C.3.

Contributors (The lead author is indicated by an asterisk (*).)

T. HAYASHI*
- Optical R&D Communications Laboratories

T. TARU
- Assistant Manager, New Business Marketing and Promotion Division

T. NAGASHIMA
- Optical R&D Communications Laboratories

O. SHIMAKAWA
- Assistant Manager, Optical R&D Communications Laboratories

T. SASAKI
- Manager, Optical R&D Communications Laboratories

E. SASAOKA
- Senior Assistant Manager, R&D General Planning Division